

Understanding the redshift evolution of the luminosity functions of Lyman- α emitters

Saumyadip Samui^{*}, Raghunathan Srianand[†], Kandaswamy Subramanian[‡]

IUCAA, Post Bag 4, Ganeshkhind, Pune 411 007, India.

3 November 2018

ABSTRACT

We present a semi-analytical model of star formation which explains simultaneously the observed UV luminosity function of high redshift Lyman break galaxies (LBGs) and luminosity functions of Lyman- α emitters. We consider both models that use the Press-Schechter (PS) and Sheth-Tormen (ST) halo mass functions to calculate the abundances of dark matter halos. The Lyman- α luminosity functions at $z \lesssim 4$ are well reproduced with only $\lesssim 10\%$ of the LBGs emitting Lyman- α lines with rest equivalent width greater than the limiting equivalent width of the narrow band surveys. However, the observed luminosity function at $z > 5$ can be reproduced only when we assume that nearly all LBGs are Lyman- α emitters. Thus it appears that $4 < z < 5$ marks the epoch when a clear change occurs in the physical properties of the high redshift galaxies. As Lyman- α escape depends on dust and gas kinematics of the inter stellar medium (ISM), this could mean that on an average the ISM at $z > 5$ could be less dusty, more clumpy and having more complex velocity field. All of these will enable easier escape of the Lyman- α photons. At $z > 5$ the observed Lyman- α luminosity function are well reproduced with the evolution in the halo mass function along with very minor evolution in the physical properties of high redshift galaxies. In particular, upto $z = 6.5$, we do not see the effect of evolving inter galactic medium (IGM) opacity on the Lyman- α escape from these galaxies.

Key words: cosmology: theory - early universe - galaxies : formation - luminosity function - high-redshift - stars

1 INTRODUCTION

Determining the star formation history of the high redshift universe is one of the major goals of ongoing observations. Available observational data mainly consists of UV luminosity functions (LFs) of high redshift Lyman break galaxies (LBGs) which can in turn give the star formation rate density of the universe. The galaxies have been identified even up to redshift $z \sim 10$ using so called photometric ‘drop-out’ technique (Bouwens et al. 2004, Hopkins & Beacom 2006, Richard et al. 2006). However, very good constraints are available only up to $z \sim 7$ (Bouwens et al 2008).

In addition to the ‘drop-out’ techniques, narrow band searches for high redshift galaxies emitting a strong Lyman- α line are successful in detecting galaxies at $3 \lesssim z \lesssim 6$ (Cowie & Hu 1998, Hu et al. 1998, Rhoads et al. 2000, Taniguchi et al. 2005, Shimashaku et al. 2006, Kashikawa et al. 2006, Murayama et al. 2007, Gronwall et al. 2007, Dawson et al 2007, Ota et al. 2008, Ouchi et al. 2008). Unlike the drop-out technique used in detecting the LBGs,

the searches for Lyman- α emitters are not biased by UV luminosity. However, the detectability depends on the Lyman- α emissivity and radiative transport. Thus these two techniques pick up galaxies with different types of selection biases. Availability of the UV luminosity functions of Lyman- α selected galaxies allows us to understand these biases and provides joint constraints on models of galaxy formation at $z > 3$.

The star formation rate is a key quantity for both UV as well as Lyman- α emission from a galaxy. Hence, it is interesting to obtain a semi-analytical model of star formation for these high redshift galaxies that can explain both these sets of observations. In our previous work by Samui, Srianand & Subramanian (2007) (hereafter Paper I) we have built a semi-analytic model of star formation taking account of several feedback processes in order to explain the observed UV luminosity functions of LBGs at $3 \leq z \leq 10$. By fitting the observed data we put constraints on the nature of the star formation in this redshift range. In Samui, Subramanian & Srianand (2009) (Paper II) we studied the effect of assumed form of the halo mass function on the results of semi-analytical galaxy formation models, in detail. As a continuation of these works, here we compute the luminosity function of Lyman- α emitters (LAEs) using the same star formation model and compare it with the three

* E-mail: samui@iucaa.ernet.in

† E-mail: anand@iucaa.ernet.in

‡ E-mail: kandu@iucaa.ernet.in

sets of available observations, which are the high redshift UV luminosity functions of LBGs and UV & Lyman- α luminosity functions of LAEs. Previous semi-analytical works on high redshift luminosity functions of Lyman- α emitters (i.e. Haiman & Spaans 1993, Thommes & Meisenheimer 2005, Le Delliou et al. 2005, 2006, Kobayashi et al 2007, Mao et al 2007, Dijkstra et al 2007, Stark et al. 2007) have considered a more limited set of currently available observations. Our present work using this more extensive set, i.e. UV and Lyman- α luminosity functions of LAEs and UV luminosity functions of LBGs in the redshift range $3 \leq z \leq 6.5$, allows us to constrain the physical properties of LAEs and their redshift evolution. We use the cosmological parameters consistent with the recent WMAP data (Dunkley et al. 2008) ($\Omega = 1$, $\Omega_m = 0.26$, $\Omega_\Lambda = 0.74$, $\Omega_b = 0.044$, $h = 0.71$, $\sigma_8 = 0.80$ and $n_s = 0.96$).

2 SEMI-ANALYTICAL MODELS

In order to compute the luminosity function of high redshift galaxies one needs to model both the star formation in an individual galaxy and the abundance of dark matter halos in which the galaxies form. We compute the abundance and formation rate of dark matter halos as a function of redshift in the framework of Lambda cold dark matter (LCDM) cosmology. For this purpose we consider two halo mass functions, the analytically motivated Press-Schechter (PS) halo mass function (Press & Schechter, 1974) and the Sheth-Tormen (ST) halo mass function (Sheth & Tormen 1999), which gives a better fit to numerical galaxy formation simulations. For the PS halo mass function, we use the formalism of Sasaki (1994) to calculate the net formation rate of halos. However, the Sasaki formalism is not easily generalisable to the other form of mass functions. Hence for the ST halo mass function, we simply take recourse to its derivative to calculate the net formation rate of dark matter halos (also see Paper II).

The star formation rate of an individual galaxy of dark matter mass M is assumed to be (Chiu & Ostriker 2000),

$$\dot{M}_{\text{SF}}(M, z, z_c) = f_* \left(\frac{\Omega_b}{\Omega_m} M \right) \frac{t(z) - t(z_c)}{\kappa^2 t_{\text{dyn}}^2(z_c)} \times \exp \left[-\frac{t(z) - t(z_c)}{\kappa t_{\text{dyn}}(z_c)} \right], \quad (1)$$

where, the amount and duration of the star formation is determined by the values of f_* and κ respectively. We can fix these two parameters by fitting the observed UV luminosity functions of high redshift LBGs (see Paper I and II for details). Further, $t(z)$ is the age of the universe; thus $t(z) - t(z_c)$ gives the age of the galaxy at z that has formed at an earlier epoch z_c , and t_{dyn} is the dynamical time at that epoch. The star formation rate is converted to luminosity at 1500 Å assuming an initial mass function (IMF) of the stars formed (see Eq. (6)-(8) of Paper I). The observed luminosity is less by a factor, η , than the actual luminosity because of the dust reddening inside the galaxy. In principle, the value of η depends on the wavelength and the functional form is governed by the nature of the dust grains. As in Paper I, we calculate the reionization history of the universe and the radiative feedback of the meta-galactic background UV radiation on the star formation in a self-consistent manner for each model (also see Thoul & Weinberg 1996, Bromm & Loeb 2002, Benson et al. 2002; Dijkstra et al. 2004). We assume a steep cut off of star formation in halos with mass $M \geq 10^{12} M_\odot$ which is attributed to AGN feedback (Bower et al. 2005; Best et al. 2006).

We compute the Lyman- α luminosity of a star forming galaxy

assuming case-B recombination. In this case, two Lyman- α photons are produced out of three hydrogen ionizing photons (Osterbrock, 1989) that are confined within the interstellar medium of the galaxy. Hence the Lyman- α luminosity produced in any star forming region is related to its star formation rate by,

$$L_{Ly\alpha} = 0.68 h \nu_\alpha (1 - f_{\text{esc}}) N_\gamma \dot{M}_{\text{SF}}. \quad (2)$$

Here, $h \nu_\alpha = 10.2$ eV and $f_{\text{esc}} = 0.1$ are the energy of a Lyman- α photon and the escape fraction of UV ionizing photons respectively. Further, N_γ is the rate of ionizing photon production per unit solar mass of star formation. This mainly depends on the initial mass function of the stars and also on the metallicity. Values of number of ionizing photons per baryon of star formation for different IMFs and different metallicities can be found in Table 1 of Paper I. The observed Lyman- α luminosity is given by

$$L_{Ly\alpha}^{\text{obs}} = f_{\text{esc}}^{Ly\alpha} L_{Ly\alpha}. \quad (3)$$

Here, $f_{\text{esc}}^{Ly\alpha}$ is the escape probability of the Lyman- α photons. This is decided by the dust optical depth, velocity field of the ISM in the galaxies and the Lyman- α optical depth due to ambient intergalactic medium around the galaxies. As Lyman- α is a resonant transition we expect the effective dust optical depth for Lyman- α in the ISM to be much larger than that for the UV continuum photons (i.e. $f_{\text{esc}}^{Ly\alpha} < 1/\eta$). However, if Lyman- α emission comes from some outflows in the star forming region (Malhotra & Rhoads 2002, Dijkstra et al. 2007a, Verhamme et al. 2008) or through inhomogeneous ISM (Neufeld 1991, Hansen & Oh 2006, Finkelstein et al. 2008, 2009) then there may not be any correlation between η and $f_{\text{esc}}^{Ly\alpha}$.

The escape fraction of Lyman- α also depends on the optical depth of the IGM in the immediate neighbourhood of the galaxy, in particular the proximate region that is affected by excess ionization by the galaxy itself. Thus the redshift evolution of $f_{\text{esc}}^{Ly\alpha}$ can be an useful probe of the reionization history of the universe (Malhotra & Rhoads 2004, Stern et al. 2005, Haiman and Cen 2005, Dijkstra, Wyithe & Haiman, 2007) and/or the redshift evolution of dust abundance (Mao et al. 2007), velocity field and gas clumping factor in galaxies.

It may be possible that all the LBGs do not have a detectable Lyman- α emission. The spectroscopic observations of LBGs by Shapley et al. (2003) show that only 25% of the LBGs at $z \sim 3$ have Lyman- α emission with rest equivalent width $W_0 \geq 20$ Å (also see Steidel et al. 2000). Also the observations of UV luminosity function of Lyman- α emitters show similar results. Hence we consider that only a fraction G_f of the entire galaxy population will be detected as Lyman- α emitters in surveys as they are usually sensitive to galaxies having Lyman- α equivalent widths above certain limiting value.

The rest frame equivalent width of the Lyman- α emission is given by

$$W_0 = L_{Ly\alpha}^{\text{obs}} / (L_{\text{cont}} / \eta) = f_{\text{esc}}^{Ly\alpha} L_{Ly\alpha} / (L_{\text{cont}} / \eta) \quad (4)$$

where L_{cont} is the continuum luminosity per unit wavelength near 1215 Å. We obtained this from the stellar synthesis code ‘Starburst99’¹ (Leitherer et al. 1999). For our continuous mode of star formation we use the same prescription as in Paper I for the UV continuum flux, to calculate the 1215 Å continuum flux. We tabulate the continuum luminosities at different wavelengths and rest frame equivalent width of Lyman- α emission in Table 1 for various

¹ <http://www.stsci.edu/science/starburst99>

Table 1. Flux at various wavelengths as predicted by ‘Starburst99’ for a continuous mode of star formation at a rate of $1 M_{\odot}/\text{yr}$. The quoted values are at the time $t = 1.4 \times 10^8$ yrs after the star formation began. We also show the equivalent width calculated at $t = 10^7$ yrs.

Model	IMF		Metal	$f_{905}^{\ddagger,1}$	$f_{1505}^{\ddagger,2}$	ratio f_{905}/f_{1505}	HI-UV ³	f_{1215}^4	EW* (\AA)	
	M_{low}	M_{up}							$1.4 \times 10^8 \text{ yrs}$	$1.0 \times 10^7 \text{ yrs}$
model1	1	100	0.050	40.12	40.37	0.57	53.13	40.44	49.4	52.4
model2	1	100	0.040	40.10	40.32	0.60	53.23	40.36	74.3	81.2
model3	1	100	0.020	40.15	40.42	0.53	53.33	40.45	75.8	87.0
model4	1	100	0.008	40.16	40.46	0.50	53.45	40.45	100.3	122.9
model5	1	100	0.004	40.18	40.48	0.51	53.50	40.46	110.6	137.9
model6	1	100	0.001	40.21	40.48	0.53	53.57	40.44	135.3	169.6
model7	1	100	0.0004	40.24	40.50	0.54	53.61	40.48	133.4	173.6
model8	0.1	100	0.0004	39.83	40.10	0.54	53.20	40.07	139.4	173.3
model9	5	100	0.0004	40.58	40.75	0.66	53.94	40.80	135.5	177.6
model10	10	100	0.0004	40.75	40.79	0.91	54.11	40.92	157.6	181.8
model11	20	100	0.0004	40.89	40.78	1.29	54.29	40.95	216.7	216.7
model12	40	100	0.0004	40.95	40.77	1.54	54.39	40.93	288.8	288.8

¹ log of flux ($\text{erg s}^{-1} \text{\AA}^{-1}$) at 905 \AA .

² log of flux ($\text{erg s}^{-1} \text{\AA}^{-1}$) at 1505 \AA .

^{\ddagger} Note that ‘Starburst99’ gives flux at 905 \AA and 1505 \AA .

³ log of no. of H I ionizing photons per sec.

⁴ log of flux ($\text{erg s}^{-1} \text{\AA}^{-1}$) at 1215 \AA .

* Equivalent widths are calculated taking $f_{esc}^{Ly\alpha} = 1$ and $f_{esc} = 0.1$ and $\eta = 1$.

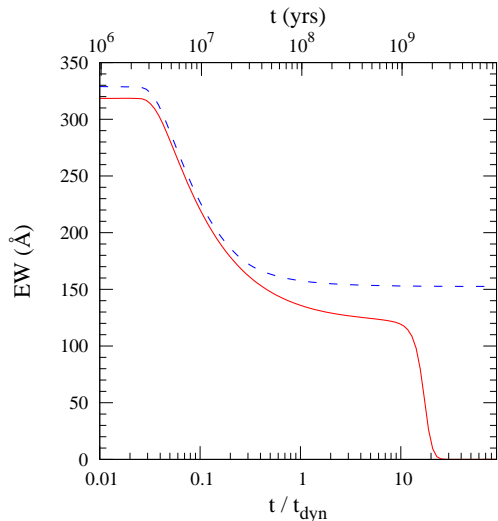


Figure 1. The time evolution of intrinsic Lyman- α equivalent width of a galaxy as predicted by our models. Solid and dashed lines are for the Salpeter IMF in the mass ranges $1 - 100 M_{\odot}$ and $10 - 100 M_{\odot}$ respectively (i.e. model7 and model10 of Table 1). We have assumed $\kappa = 1$. The dynamical time (t_{dyn}) depends on redshift of collapse (z_c). For example, at $z_c = 10, 5$ and 3 , $t_{dyn} = 8.8 \times 10^7, 2.2 \times 10^8$ and 4×10^8 yrs respectively. We also show the actual time that corresponds to $z_c = 10$ on the top axis.

physical parameter related to the nature of the star formation for a continuous constant star formation model as obtained from ‘Starburst99’ at the time $t = 1.4 \times 10^8$ yrs after the star formation began. We also quote the equivalent width calculated at $t = 10^7$ yrs. Note that for a constant continuous star formation model, the number of high mass star remain constant after typical life time of OB stars that dominate in $L_{Ly\alpha}$. Hence, the equivalent width decreases with time as contribution from the low mass stars to L_{cont} continuously adds up.

In our model the Lyman- α equivalent width of a galaxy is independent of its mass as both Lyman continuum as well as line flux would scale with mass. It depends on the value of κt_{dyn} and most importantly the values of η and $f_{esc}^{Ly\alpha}$. It also depends on the value of f_{esc} , the escape fraction of the ionizing photons. In Fig. 1 we show the time evolution of the intrinsic rest frame equivalent width of a galaxy as predicted by our models. The observed equivalent width would be scaled by a factor $\eta f_{esc}^{Ly\alpha}$. We also assume a Salpeter IMF in the mass range $1 - 100 M_{\odot}$ (solid line) and $10 - 100 M_{\odot}$ (dashed line). As can be seen from Table 1 as well as from Fig. 1, the intrinsic equivalent width depends on the assumed IMF. Note that through out this work we will use $\kappa = 1$ and Salpeter IMF with the mass range $1 - 100 M_{\odot}$ with metallicity 0.0004 (i.e. model7 of Table 1).

Note that we have mainly three sets of observations that can be used to constrain our model parameters. These are (i) UV luminosity function of LBGs, (ii) Lyman- α luminosity function of Lyman- α emitters and (iii) UV luminosity function of Lyman- α emitters. Along with these we have the information about the equivalent width distribution of the LAEs. The first set of observations can be used to constrain f_*/η combination. The second set can be used to constrain $f_* f_{esc}^{Ly\alpha}$ and the last one can be used to obtain G_f . Then we will be able to calculate the mean W_0 . The spread in the equivalent width of the detected galaxies will come in two ways: (i) distribution in η and $f_{esc}^{Ly\alpha}$ and (ii) the spread in their ages. Since in our model we assume only the average value for both η and $f_{esc}^{Ly\alpha}$, we will have distribution in W_0 only coming from the spread in the ages of detected galaxies. We show this distribution in the following section while discussing our results.

3 LUMINOSITY FUNCTIONS

In Fig. 2 we compare our model predictions for both UV and Lyman- α luminosity functions with the observed data points. For each redshift bin we have used the most recent measurement of the

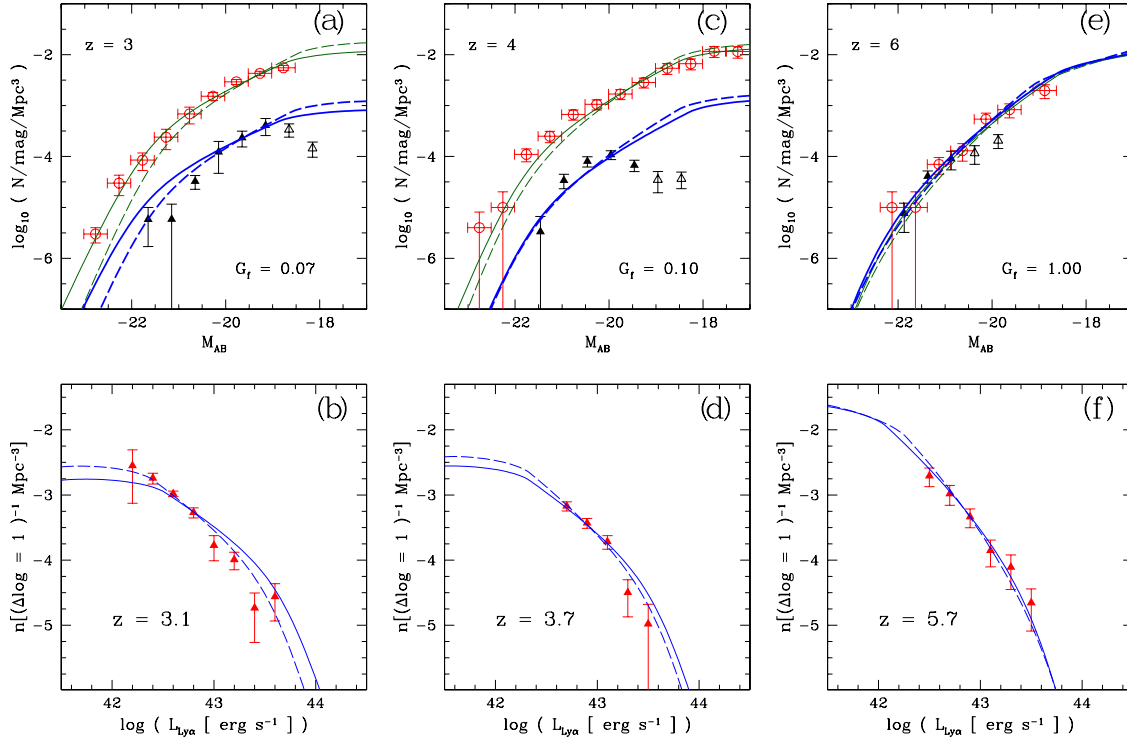


Figure 2. Top panels: The predicted UV luminosity functions of LBGs (thin green lines) and LAEs (thick blue lines) at $z = 3, 4$ and 6 along with the observed data points. The observationally determined UV luminosity functions of LBGs are taken from Reddy & Steidel (2008) (open red circle at $z = 3$) and Bouwens et al (2007) (open red circles at $z = 4$ and $z = 6$). The black filled and open triangles are observed data points of UV LFs of LAEs from Ouchi et al. (2008) for the reliable and less reliable points respectively. We show our model predictions for both Press-Schechter (dashed lines) and Sheth-Tormen (solid lines) halo mass functions. Bottom panels: The predicted Lyman- α LF of LAEs at $z = 3.1, 3.7$ and 5.7 . The observed data points (red filled triangles) are from Ouchi et al. (2008). The solid lines are for the models with the Sheth-Tormen mass function where as dashed lines are for the Press-Schechter mass function.

Table 2. Comparison of model predictions between the PS and ST mass functions.

z	PS Mass function				ST Mass function			
	f_*/η^\dagger	G_f	$f_* f_{esc}^{Ly\alpha\ddagger}$	EW* (\AA)	f_*/η^\dagger	G_f	$f_* f_{esc}^{Ly\alpha\ddagger}$	EW* (\AA)
3.1	0.044(3.90)	0.07	0.059 ± 0.011 (0.95)	179	0.055(0.97)	0.07	0.076 ± 0.011 (2.49)	183
3.7	0.046(2.32)	0.10	0.051 ± 0.014 (0.68)	148	0.042(1.09)	0.10	0.050 ± 0.015 (1.08)	159
5.7	0.081(1.19)	1.00	0.044 ± 0.017 (0.91)	72	0.050(0.63)	1.00	0.028 ± 0.021 (0.42)	75
6.5	-	1.00	0.054 ± 0.012 (2.30)	-	-	1.00	0.031 ± 0.015 (2.32)	-

\dagger obtained using χ^2 minimization and also corrected for dust opacity at $\lambda = 1500 \text{ \AA}$;

the χ^2 per degree of freedom are given in bracket (see Paper II for details).

\ddagger values indicated inside the bracket are best fit χ^2 per degree of freedom.

* the average equivalent width is calculated at $t = 10^8$ yrs.

UV luminosity function of LBGs that covers a wide range in luminosity. Below we provide details of observational data used in each redshift bins. Luminosity functions of LAEs are taken from Ouchi et al. (2008). The solid and dashed lines are our model predictions using ST and PS halo mass functions respectively.

At a particular redshift, we first fit the observed UV luminosity functions of LBGs by adjusting f_*/η . For this we use χ^2 minimization technique (see Paper II for details). Then we fit the observed UV luminosity function of LAEs by changing G_f and keeping same f_*/η obtained for the nearest available redshift. Note that, we did not try to get G_f through χ^2 minimization as there are

only few data points in the observed luminosity function (also there are issues related to the completeness of the samples). Finally we match our model predictions with observed Lyman- α luminosity function at the same redshift by adjusting $f_* f_{esc}^{Ly\alpha}$ and keeping G_f fixed. This is also done using χ^2 minimization. In Table 2 we summarize the best fit parameters along with the χ^2 vales at different redshifts for models with both PS and ST mass functions. Below we describe these results for specific redshifts.

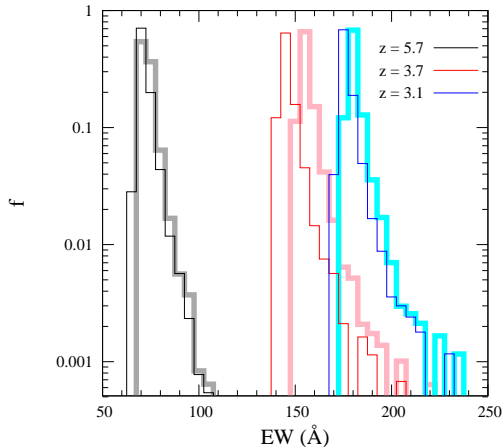


Figure 3. Distribution of Lyman- α equivalent width as predicted by our model at $z = 3.1, 3.7$ and 5.7 . The thin lines are for the models that assume the PS halo mass function where as the thick lines are for the models with the ST mass function. Note that, here the spread in EW only comes from different ages of galaxies contributing to the luminosity function. In reality more spread is expected from the spread in values of η and $f_{esc}^{Ly\alpha}$.

3.1 Luminosity functions at $z \sim 3$

At $z \sim 3$ we have all the three observed luminosity functions and the data are quite well established, i.e. different groups have confirmed the data by different methods. For $z \sim 3$ we use the observed UV luminosity function of LBGs given by Reddy & Steidel (2008) which covers the low luminosity end well. We show in the left most panels of Fig. 2 (panel (a) and (b)), both UV and Lyman- α luminosity functions at $z \sim 3$ as predicted by our model along with the observed data points. The best fit model parameters are given in Table 2. In panel (a) of Fig. 2, the set of thin curves in the top are the predictions of UV luminosity functions of LBGs.

A good agreement with the observed UV luminosity function of LBGs is obtained for $f_*/\eta = 0.044 \pm 0.001$ and 0.055 ± 0.001 for models with the PS and ST mass functions respectively. The corresponding reduced χ^2 for these fits are 3.9 and 0.97. Thus the shape of the observed UV luminosity function of the LBGs is better reproduced by the model with the ST halo mass function. We fit the UV luminosity function of the Lyman- α emitters by multiplying the UV LF of LBGs with a fraction G_f . As mentioned earlier, we did not try to get G_f through χ^2 minimization. The observed data points are well reproduced for $G_f = 0.07$ with same f_*/η . These curves are also shown in the figure by the thick blue lines (the bottom set of curves in panel (a)) for both PS and ST mass functions. The declining trend in the UV luminosity function of Lyman- α emitters seen in the low luminosity end (open triangles) is mainly due to incompleteness. Apart from these points other data points do not require luminosity dependent G_f . This is consistent with our implicit assumption that G_f is independent of halo mass (or galaxy luminosity).

The value of G_f is in agreement with the measurements of Shapley et al (2003) where they found that the fraction of LBGs having Lyman- α emission with equivalent width $W_0 \geq 60 \text{ \AA}$ is $\sim 8\%$ (see their Fig. 8). Note that the sample of LAEs of Ouchi et al (2008) at $z = 3.1$ has $W_0 \geq 60 \text{ \AA}$. Hence our results are consistent with both these observations. From the fact that G_f matches with the prediction from fig. 8 of Shapley et al. (2003) we can conclude that both the techniques of detecting $z \sim 3$ galaxies appear to pick a subset of the same parent population of galaxies.

We now turn to Lyman- α LF of LAEs. We show this in panel (b) of Fig. 2 along with the observational data taken from Ouchi et al. (2008). To fit the Lyman- α luminosity function, only free parameter is $f_* f_{esc}^{Ly\alpha}$ as G_f has already been fixed by fitting the UV luminosity function of the LAEs. The best fit with the observational data are obtained with $f_* f_{esc}^{Ly\alpha} = 0.059 \pm 0.011$ and 0.076 ± 0.011 for the PS and ST mass functions respectively. The corresponding best fit χ^2 are 0.95 and 2.49. If we consider $\eta = 4.5$ as obtained by Reddy et al. (2006) then we have $f_{esc}^{Ly\alpha} = 0.29$ and 0.30 respectively for the models with the PS and ST mass functions. Taking $\eta = 4.5$ also implies $f_* = 0.20$ and $f_* = 0.25$ for the models with the PS and ST mass functions respectively.

We now calculate the average rest frame equivalent width of the Lyman- α emission of the star forming galaxies that are contributing to the luminosity function. Note that for given values of f_*/η and $f_* f_{esc}^{Ly\alpha}$, the equivalent width is solely determined from the IMF we assume. This can be easily understood if we rewrite Eq. 4 as

$$W_0 = \frac{L_{Ly\alpha}(f_* f_{esc}^{Ly\alpha})}{L_{cont}(f_*/\eta)}. \quad (5)$$

The ratio $L_{Ly\alpha}/L_{cont}$ depends on the IMF and the metallicity of the gas (see Table 1) and f_*/η and $f_* f_{esc}^{Ly\alpha}$ come from the fit. Therefore, fitting simultaneously the UV and Lyman- α luminosity functions uniquely specify the average equivalent width of the Lyman- α emission line. For the fit presented in panels (a) and (b) of Fig. 2 the average equivalent widths are 179 \AA and 183 \AA for the models with the PS and ST mass functions respectively. Note that ‘ η ’ reflects extinction at $\lambda \sim 1500 \text{ \AA}$; the relative extinction at $\lambda = 1215 \text{ \AA}$ will be higher than that at $\lambda = 1500 \text{ \AA}$. Therefore, the actual equivalent width will be higher depending upon the adopted extinction correction. The Lyman- α rest equivalent width distribution predicted for the best fit model parameters is shown in Fig. 3. Note that the spread in η and $f_{esc}^{Ly\alpha}$ around their best fitted values will make this distribution spread over wider equivalent width range. Hence, one should not directly compare this histogram with observations although the mean value itself is relevant. In all results presented here we use a lower mass cut off of $1 M_\odot$ in the assumed IMF. Increasing this to $\geq 10 M_\odot$ to mimic a top-heavy IMF would increase the predicted equivalent width by a factor ~ 1.4 (see Fig. 1).

3.2 Luminosity functions at $z \sim 4$

We show our model prediction as well as the observed data points at $z \sim 4$ in panel (c) and (d) of Fig. 2. The observed UV luminosity function of LBGs at $z = 4$ is taken from Bouwens et al. (2007). The luminosity function of Lyman- α emitters is at $z = 3.7$ and we compare this with UV luminosity function of LBGs at $z = 4$. We see from our model predictions that there is no significant change in the properties of the galaxies from $z \sim 3$ to $z \sim 4$. The UV luminosity function of LBGs can be well fitted with $f_*/\eta = 0.046 \pm 0.001$ and 0.042 ± 0.001 with all other parameters being same as at $z = 3$ for the models using the PS and ST mass functions respectively (see Table 2). The corresponding reduced χ^2 are 2.32 and 1.09. Thus, even for this redshift bin the model with the ST mass function provides a better fit to the observed data. If we assume $\eta = 4.5$, we get $f_* = 0.21$ and 0.19 for the models with PS and ST mass functions respectively.

In order to fit the observed UV luminosity function of LAEs of Ouchi et al. (2008) at $z = 3.7$ we need $G_f = 0.1$. Comparing the values of G_f , we conclude that there is no strong evolution

in the percentage of LBGs showing up as LAEs from $z = 3$ to $z = 4$. Assuming no redshift evolution in the equivalent width distribution of Lyman- α and taking the limiting rest equivalent width of 45 \AA (as in Ouchi et al. 2008) we estimate $G_f \sim 0.1$ from the Fig. 8 of Shapley et al. (2003). However, Reddy et al. (2008) report an evolution in the Lyman- α equivalent width distribution of LBGs between $1.9 \leq z \leq 3.4$. Continuation of this trend to higher redshifts will mean G_f more than 10%. Our model predictions match reasonably well with these observational predictions given the error in measurements.

The good agreement with the data of Lyman- α LF at $z = 3.7$ (taken from Ouchi et al. 2008) are obtained for $f_* f_{esc}^{Ly\alpha} = 0.051 \pm 0.014$ for the model with the PS mass function with best fit $\chi^2/\text{dof} = 0.68$. The mean Lyman- α equivalent width of the LAEs as predicted from this model is 148 \AA . For the model with the ST mass function one needs $f_* f_{esc}^{Ly\alpha} = 0.050 \pm 0.015$ (with best fit $\chi^2/\text{dof} = 1.08$) and the average equivalent width predicted by this model is 183 \AA . The Lyman- α rest equivalent width distribution predicted for the best fit model parameters is shown in Fig. 3. For $\eta = 4.5$ we get $f_{esc}^{Ly\alpha} = 0.25$ and 0.26 for PS and ST mass functions respectively. These values are consistent with that we derived for $z \sim 3$. Therefore with no or minor evolutions in the physical conditions in the Lyman break galaxies our models reproduce the observed luminosity function for $3 \leq z \leq 4$. However, from Fig. 3 it is clear that our models predict a mild decrease in the rest equivalent width of Lyman- α with increasing redshift.

3.3 Luminosity functions at $z \sim 6$

In the panels (e) and (f) of Fig. 2, we show our model prediction of luminosity functions at $z \sim 6$. The observed UV luminosity functions of LBGs at $z = 6$ are taken from Bouwens et al. (2007). First, the required values of f_*/η are 0.081 ± 0.001 and 0.050 ± 0.001 for the model with the PS and ST mass functions respectively. The corresponding reduced χ^2 are 1.19 and 0.63 suggesting both PS and ST mass functions produce good fit to the data. We need $G_f = 1.0$ to reproduce the UV luminosity function of LAEs at this redshift. Hence 100% of the LBGs are detected as LAEs at $z \sim 6$. This is considerably different from $z = 3$ or 4 where only $\sim 10\%$ of LBGs are detectable as LAEs. Assuming no redshift evolution in the equivalent width distribution of Lyman- α and taking the limiting rest equivalent width of 25 \AA (as in Ouchi et al. 2008) we estimate $G_f \sim 0.25$ from the Fig. 8 of Shapley et al. (2003). This means that the physical properties related to the Lyman- α emission have changed considerably from $z = 3.7$ to $z = 5.7$. This conclusion depends very much on the accuracy of the observed luminosity functions. While data of Shimasaku et al. (2006) is consistent with that of Ouchi et al (2008), there are some discrepancies in the fraction of Lyman break selected galaxies that are also Lyman- α emitters (see Rhoads et al. 2003; Hu et al. 2004; Ajiki et al. 2003 and Dow-Hygelund et al. 2007). We will come back to this issue in the discussion section. As we have been using Ouchi et al's data in all redshift bins we base our conclusions on their data.

We show our model predictions for the Lyman- α luminosity function of LAEs at $z = 5.7$ in panel (f) of Fig. 2. The observed data points are taken from Ouchi et al. (2008). To fit the observed Lyman- α LF one needs $f_* f_{esc}^{Ly\alpha} = 0.044 \pm 0.017$ for the model using the PS mass function. The best fit χ^2 per degree of freedom is 0.91. Therefore, even though the fraction of LAEs has increased considerably from $z = 3$ to $z = 6$, the value of $f_* f_{esc}^{Ly\alpha}$ in the galaxies identified as Lyman- α emitters which characterises the Lyman- α escape (for fixed f_*) has changed negligibly (within

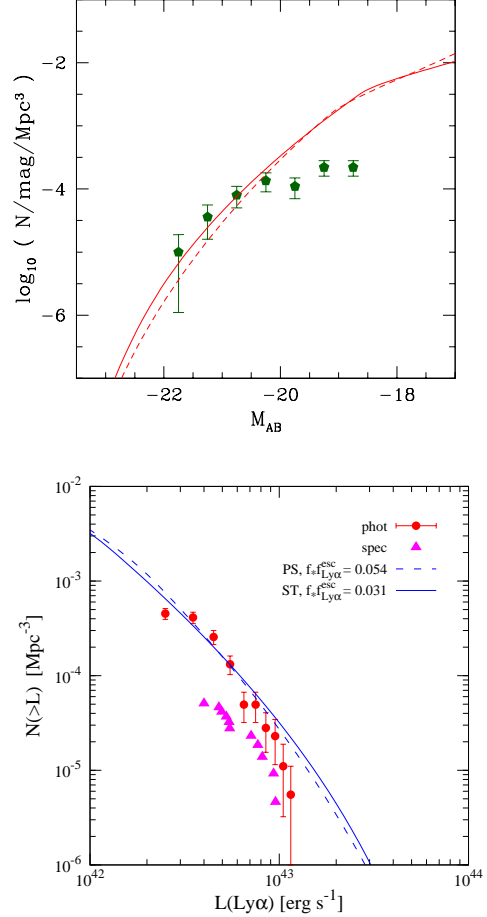


Figure 4. *upper panel* : The UV luminosity functions of Lyman- α emitters at $z = 6.5$. The observed data are from Kashikawa et al., 2006. The predicted UV luminosity functions of LBGs at $z = 6.5$ for the ST and PS halo mass functions are shown by solid and dashed lines respectively. We take the values of f_*/η that fits the UV luminosity functions at $z = 6$. *lower panel* : The cumulative Lyman- α LF at $z = 6.5$. The solid line is for the ST mass function and dashed is for PS mass function. The spectroscopic (filled triangles) and photometric (filled circles) data are taken from Kashikawa et al. (2006). The model parameters are adjusted to fit the luminosity function obtained from the photometric data.

the uncertainty of the best fit values). However, this is only true for the model with the PS mass function. Model that uses the ST mass function predicts a change in the escape of the Lyman- α photons at $< 3\sigma$ level. For this model, the best fit is obtained with $f_* f_{esc}^{Ly\alpha} = 0.028 \pm 0.021$ (with best fit $\chi^2/\text{dof} = 0.42$). The calculated mean equivalent widths are 72 \AA and 75 \AA for model with the PS and ST mass functions respectively. The predicted rest equivalent width distribution is shown in Fig. 3. As noted above we see a decrease in the average equivalent width with increasing redshift.

3.4 Cumulative luminosity function at $z = 6.5$

Fan et al. (2006) have shown, based on the spectra of QSOs, that there is a significant increase in the IGM neutral fraction at $z \gtrsim 6$. As Lyman- α escape also depends on the IGM opacity one expects a significant change in the Lyman- α luminosity function at $z \gtrsim 6$. Kashikawa et al. (2006) have given the integrated Lyman- α lumi-

nosity function and the UV luminosity function of Lyman- α emitters at $z = 6.5$. The observed data and our model predictions are compared in Fig. 4. We use $f_*/\eta = 0.081$ and 0.050 respectively for the models with the PS and ST mass functions. These are the best fitted values for $z \sim 6$ UV luminosity function of LBGs. They provide a good fit to the observed UV luminosity function of LAEs at $z \sim 6$ for $G_f = 1$. Our model predictions of the Lyman- α luminosity function match reasonably well with the observed data (bottom panel in Fig. 4). The good agreement with the data is obtained for $f_* f_{esc}^{Ly\alpha} = 0.054 \pm 0.012$ and 0.031 ± 0.015 for the PS and ST mass function respectively. The corresponding best fit χ^2 per degree of freedom are 2.30 and 2.32. These two values are similar to those at $z = 5.7$. Hence, we conclude that the evolution in the dark matter halo mass function is sufficient to explain the observed evolution in the Lyman- α LF from $z = 5.7$ to $z = 6.5$ without any major changes in other physical properties related to the star formation in the high redshift galaxies.

4 CONCLUSION AND DISCUSSION

We have built a semi-analytical model of star formation for high redshift galaxies which simultaneously reproduces the observed UV luminosity functions of LBGs and LAEs and the Lyman- α luminosity function of LAEs in the redshift range $3 \leq z \leq 6.5$. We fit the UV luminosity functions of LBGs by changing f_*/η while we adjust G_f , the fraction of LBGs detected as LAEs, to match the UV luminosity functions of LAEs. Finally to fit the Lyman- α LFs of LAEs we vary $f_* f_{esc}^{Ly\alpha}$. The best fit values of our model parameter at different redshifts allow us to probe the redshift evolution of properties of galaxies. In our models we make an implicit assumption that the Lyman- α emitters are a subset of a parent population of normal galaxies detected through Lyman break technique.

Within the observational uncertainties, we are able to reproduce the observed UV luminosity functions of Lyman- α emitters by simply scaling the best fitted UV luminosity functions of LBGs by a constant factor G_f . This basically means that at a given z the fraction of LBGs that are seen as Lyman- α emitters is independent of the UV luminosity of galaxies and mass of the dark matter halos. Improving the errors in the UV luminosity functions of Lyman- α emitters will allow us to investigate the possible dependence of G_f on the mass of the galaxies.

The most interesting results from our study is the redshift evolution of G_f . We showed that for $z \sim 3.1$ the well measured fraction of Lyman- α emitters among the LBGs are consistent with the G_f we require to fit the three luminosity function at this redshift. Our model fits to the observations clearly show a strong evolution in G_f between $z < 4$ and $z > 5$. Physically G_f at any given redshift will be given by the distribution in the Lyman- α escape among the population of LBGs. This will be governed by E(B-V), line of sight H I column density, velocity field in the Lyman- α emitting region and/or the duty cycle of the burst of star formation. It is interesting to note that even if there is absolutely no change in the distribution of Lyman- α equivalent width (absorption as well as emission) as a function of redshift one expects G_f to increase with z mainly because of the decrease in the limiting rest equivalent width of Lyman- α emission in Ouchi et al's. (2008) survey. For example, based on Fig. 8 of Shapely et al. we expect G_f to be 0.25 at $z \sim 6.0$. From, Fan et al. (2006) we notice that the IGM transmission decreases by at least a factor 3 between $z = 3.1$ and $z = 5.7$ due to Gunn-Peterson optical depth. The actual change in the IGM optical depth in the proximity of the Lyman- α emitter is difficult

to quantify as it depends on the ionization efficiency of the galaxy. Therefore, we expect $G_f \lesssim 0.25$ if the properties of LBGs do not change between $z \sim 3.1$ and $z \sim 5.7$. Thus our results giving $G_f = 1.0$ at $z \sim 6$ strongly support an evolution in the physical properties of these galaxies with redshift.

Ouchi et al. (2008) provides luminosity functions only at $z = 3.1, 3.7$ and 5.7 . From our analysis we see a sudden jump in G_f between $z = 3.7$ and $z = 5.7$. In order to explore whether this change is gradual or not, we consider few other observations in the intermediate redshift. At $z = 4.5$ Dawson et al. (2007) have measured Lyman- α luminosity function of LAEs. In absence of UV luminosity function of their sample we are unable to follow the same procedure as earlier. However, we notice that values of G_f and $f_{esc}^{Ly\alpha}$ that fit the Lyman- α LF of Ouchi's sample at $z = 3.7$ produce a good fit to the Dawson et al. data where as using the best fit parameters at $z = 5.7$ over produces the abundance of $z = 4.5$ Lyman- α emitters. There are two independent measurements of luminosity functions of LAEs available at $z = 4.86$: one by Ouchi et al. (2003) and other by Shioya et al (2008). Ouchi et al. (2003) covers the low luminosity end of the LF ($5 \times 10^{41} < L_{Ly\alpha}(\text{erg s}^{-1}) < 2 \times 10^{43}$) where as Shioya et al (2008) covers the high end ($8 \times 10^{42} < L_{Ly\alpha}(\text{erg s}^{-1}) < 4 \times 10^{43}$) with slight overlap between them. The Ouchi et al. (2003) measurements are consistent with $G_f = 0.1$. However, if we also consider Shioya et al (2008) data, G_f could be as large as 0.3. Note that the completeness of the sample is always an issue in this case. Hence more observations are needed in this redshift range in order to probe in detail how G_f increases to unity by $z = 5.7$.

Unlike at $z \sim 3.1$, the luminosity function of Lyman- α emitters obtained by different groups for $z \sim 5.7$ disagree up to a factor 5 (see Rhoads et al. 2003; Hu et al 2004; Ajiki et al. 2003; Murayama et al. 2007; Shimasaku et al. 2006; and Ouchi et al. 2008). The difference could be due to differences in the colour selection criteria used in the narrow band survey and the depth of the broad band photometry. Dow-Hygelund et al. (2007) have found that only 30% of the Lyman break galaxies at $z \sim 6$ selected through i-dropout selection show Lyman- α emission with rest equivalent width $\geq 20 \text{ \AA}$. It is also important to remember that while the narrow band imaging picks object within very narrow redshift range the broad band colour techniques pick objects over a much wider redshift range. Incompleteness levels in these two types of surveys are also very different. Dow-Hygelund et al. (2007) have shown that the i-band selection misses considerable number of Lyman- α emitters at $z < 5.8$. On the other hand, the narrow band technique of Ouchi et al (2008) picks object at $z = 5.70 \pm 0.01$. After taking into account this effect Dow-Hygelund et al (2007) conclude that up to 40% of the i-dropout galaxies could be Lyman- α emitters. From our models we find the redshift evolution between the mean z of LBGs and LAEs will account for an additional 10% increase in G_f . Even after taking into account all these effects one needs G_f to be factor 2 higher to explain the available observed luminosity functions. Thus we can conclude that there is an increase in G_f as a function of z but to get the actual amount we need lot more observations at $z > 5$. Recent results from the narrow band survey of Lyman- α emitters at $z \sim 4.7$ by Shioya et al (2009) are also consistent with increasing value of G_f with increasing z . As Lyman- α escape depends on the amount of dust and gas kinematics, the higher value of G_f implies that on an average the ISM of $z > 5$ galaxies are less dusty, more clumpy and having complex velocity field making the escape of Lyman- α photons easier.

Further, the evolution in the observed Lyman- α LF at $z \geq 5.7$ can be understood as evolution in the number density of the dark

matter halos arising from the structure formation model with modest change in the physical properties of these galaxies. This is independent of the form of the halo mass function we assume. Dijkstra et al. (2007) have arrived at same conclusion in the evolution of luminosity functions for $z \geq 5.7$ while considering no evolution in the IGM transitivity in this redshift range.

Our best fit models at different redshifts show that average Lyman- α equivalent width decreases with increasing redshift. This is contrary to some preliminary observational results that suggest an increase of equivalent width with increasing redshift (Grove et al. 2009). This result needs to be confirmed with larger number of spectroscopic data. In our model it is possible to get such a trend by allowing the initial stellar mass function to vary with redshift (see Fig. 1). Also, relaxing our assumption that the equivalent width is independent of galaxy mass will have some effect on the equivalent width distribution. Indeed such mass dependence of equivalent width distribution is indicated by observations of Ando et al. (2006).

There are a number of other attempts to fit the UV and Lyman- α luminosity functions using galaxy formation models. Kobayashi et al. (2007) using their hierarchical galaxy formation models fitted the luminosity function of Lyman- α emitters by varying the escape fraction. However, according to their models all LBGs would be detected as Lyman- α emitters. Mao et al (2008) fitted luminosity functions using semi-analytic models that compute E(B-V) and relate it to the escape fraction of Lyman- α photons. In this model preferably low metallicity dust free galaxies will be seen as Lyman- α emitters. However, recent observations suggest that the Lyman- α emitters need not be confined to primordial low dust populations (Pentericci et al. 2008; also see Scannapieco et al. 2003, Fynbo et al. 2003, Dawson et al. 2007). Nagamine et al (2008) used the hierarchical structure formation models to fit the Lyman- α emitters assuming a normal galaxy is a Lyman- α emitter for a brief period of time (duty cycle argument). They find the duty cycle increases with increasing redshift as we find for G_f .

It is important to realize that high redshift luminosity functions are based on deep field observations covering small volumes. The effect of cosmic variance may be large. The UV luminosity functions used here for LBGs are mainly based on photometric data with large redshift uncertainty. Therefore, more observations are needed to get a clearer picture on the evolution of physical properties of the galaxies. In the case of modelling, one requires a clear physical model for G_f . It is possible that simple ideas of duty cycle based on dust properties may not be sufficient since the velocity field in the Lyman- α emitting regions may play an important role. Indeed, all the high- z LBGs show signatures of outflows that can enable easy transport of Lyman- α photons. Thus, physical understanding of G_f based on a dynamical model (e.g Verhamme et al. 2008) that will also fit the luminosity functions is the next step in this subject. Such models may also explain the observed wide spread in the rest equivalent width distribution.

ACKNOWLEDGEMENTS

We thank an anonymous referee for useful comments that has helped in improving our paper. We thank Masami Ouchi for providing data on Lyman- α luminosity functions at $z = 3.1, 3.7$ and 5.7 as well as some useful discussion. We also thank Nobunari Kashikawa for providing the observational data at $z = 6.5$. SS thanks CSIR, India for the grant award No. 9/545(23)/2003-EMR-I.

REFERENCES

- Ajiki, M. et al., 2003, *AJ*, 126, 2091
 Ando, M., Ohta, K., Iwata, I., Akiyama, M., Aoki, K., Tamura, N., 2006, *ApJ*, 645, 9
 Benson, A. J., Lacey, C. G., Baugh, C. M., Cole, S., Frenk, C. S., 2002, *MNRAS*, 333, 156
 Best, P. N., Kaiser, C. R., Heckman, T. M., Kuffmann, G., 2006, *MNRAS*, 368, L67
 Bouwens R. J. et al., 2004 *ApJ*, 616, L79
 Bouwens, R. J., Illingworth, G. D., Franx, M., Ford, H., 2008, *ApJ*, 686, 230
 Bouwens, R. J., Illingworth, G. D., Franx, M., Ford, H., 2007, *ApJ*, 670, 928
 Bower, R. G., Benson, A. J., Malbon, R., Heilly, J. C., Frenk, C. S., Baugh, C. M., Cole, S., Lacey, C. G., 2006, *MNRAS*, 370, 645
 Bromm, V., Loeb, A., 2002, *ApJ*, 575, 111
 Cowie, L. L., & Hu, E. M. 1998, *AJ*, 115, 1319
 Chiu W. A., Ostriker J. P., 2000, *ApJ*, 534, 507
 Dawson, S., Rhoads, J. E., Malhotra, S., Stern, D., Wang, J., Dey, A., Spinrad, H., Jannuzi, B. T., 2007, *ApJ*, 671, 1227
 Dijkstra, M., Haiman, Z., Rees, M., Weinberg, D. H., 2004, *ApJ*, 601, 666
 Dijkstra, M., Lidz, A. & Wyithe, J. S. B., 2007, *MNRAS*, 377, 1175
 Dijkstra, M., Wyithe, J. S. B., Haiman, Z., 2007, *MNRAS*, 379, 253
 Dow-Hygelund, C. C. et al., 2007, *ApJ*, 660, 47
 Dunkley, J. et al., 2008, arXiv:0803.0586
 Fan, X., Strauss, M. A., Richards, G. T. et al., 2006, *AJ*, 131, 1203
 Finkelstein, S. L., Rhoads, J. E., Malhotra, S., Grogan, N., Wang, J., 2008, *ApJ*, 678, 655
 Finkelstein, S. L., Rhoads, J. E., Malhotra, S., Grogan, N., 2009, *ApJ*, 691, 465
 Gronwall, C., et al. 2007, *ApJ*, 667, 79
 Grove, L. F., Fynbo, J. P. U., Ledoux, C., Limousin, M., Moller, P., Nilsson, K., Thomsen, B., 2009, arXiv:0901.3845
 Haiman, Z., Cen, R., 2005, *ApJ*, 623, 627
 Haiman, Z., Spaans, M., 1999, *ApJ*, 518, 138
 Hansen, M., Oh, S. P., 2006, *MNRAS*, 367, 979
 Hopkins A. M., Beacom J. F., 2006, *ApJ*, 651, 142
 Hu, E. M., Cowie, L. L., & McMahon, R. G. 1998, *ApJ*, 502, L99
 Hu, E. M., Cowie, L. L., Capak, P., McMahon, R. G., Hayashino, T., Komiyama, Y., 2004, *AJ*, 127, 563
 Iwata, I., Ohta, K., Tamura, N., Akiyama, M., Aoki, K., Ando, M., Kiuchi, G., Sawicki, M., 2007, *MNRAS*, 376, 1557
 Kashikawa, N. et al. 2006, *ApJ*, 637, 631
 Kobayashi, M. A. R., Totani, T. & Nagashima, M., 2007, *ApJ* 670, 919
 Le Delliou, M., Lacey, C., Baugh, C. M., Guiderdoni, B., Bacon, R., Courtois, H., Sousbie, T., & Morris, S. L. 2005, *MNRAS*, 357, L11
 Le Delliou, M., Lacey, C. G., Baugh, C. M., & Morris, S. L. 2006, *MNRAS*, 365, 712
 Leitherer, C., et al., 1999, *ApJS*, 123, 3
 Malhotra, S., Rhoads, J. E., 2002, *ApJ*, 565, 71
 Malhotra, S., Rhoads, J. E., 2004, *ApJ*, 617, 5
 Mao, J., Lapi, A., Granato, G. L., de Zotti, G., Danese, L., 2007, *ApJ*, 667, 655
 Murayama, T., et al. 2007, *ApJS*, 172, 523
 Nagamine, K., Ouchi, M., Springel, V., Hernquist, L., 2008, arXiv:0802.0228
 Neufeld, D. A., 1991, *ApJ*, 370, 85
 Osterbrock, D. E. 1989, *Astrophysics of Gaseous Nebulae and Active Galactic Nuclei* (Mill Valley: University Science Books)
 Ota, K. et al., 2008, *ApJ*, 677, 12
 Ouchi et al., 2008, *ApJS*, 176, 301
 Pentericci, L., Grazian, A., Fontana, A., Castellano, M., Giallongo, E., Salimbeni, S., Santini, P., 2008, arXiv:0811.1861
 Press W. H., Schechter P., 1974, *ApJ*, 187, 425
 Reddy, N. A., Steidel, C. C., Fadda, D., Yan, L., Pettini, M., Shapley, A. E., Erb, D. K., Adelberger, K. L., 2006, *ApJ*, 644, 792
 Reddy, N. A., Steidel, C. C., 2008, arXiv:0810.2788

- Rhoads, J. E., Malhotra, S., Dey, A., Stern, D., Spinrad, H., & Jannuzi, B. T. 2000, *ApJ*, 545, L85
- Rhoads, J. E. et al., 2003, *ApJ*, 125, 1006
- Richard R., Pello R., Schaere D., Le Borgne J. F., Kneib J. P., 2006, *A&A*, 456, 861
- Samui, S., Srianand, R., Subramanian, K., 2007, *MNRAS*, 377, 285
- Samui, S., Subramanian, K., Srianand, R., 2009, *NewA*, 14, 591
- Sasaki S., 1994, *PASJ*, 46, 427
- Scannapieco, E., Schneider, R., Ferrara, A., 2003, *ApJ*, 589, 35
- Shapley, A. E., Steidel, C. C., Pettini, M., Adelberger, K. L., 2003, *ApJ*, 588, 65
- Sheth R. K., Tormen G., 1999, *MNRAS*, 308, 119 (ST)
- Shimasaku, K., et al. 2006, *PASJ*, 58, 313
- Shioya, Y., et al., 2009, *arXiv:0901.4627*
- Stark, D. P., Loeb, A., & Ellis, R. S. 2007, *ApJ*, 668, 627
- Steidel, C. C., Adelberger, K. L., Shapley, A. E., Pettini, M., Dickinson, M., Giavalisco, M., 2000, *ApJ*, 532, 170
- Steidel, C. C., Adelberger, K. L., Shapley, A. E., Pettini, M., Dickinson, M., Giavalisco, M., 2003, *ApJ*, 592, 728
- Stern, D., Yost, S. A., Eckart, M. E., Harrison, F. A., Helfand, D. J., Djorgovski, S. G., Malhotra, S., Rhoads, J. E., 2005, *ApJ*, 619, 12
- Taniguchi, Y., et al. 2005, *PASJ*, 57, 165
- Thommes, E., Meisenheimer, K., 2005, *A&A*, 430, 877
- Thoul A. A., Weinberg D. H., 1996, *ApJ*, 465, 608
- Verhamme, A., Schaerer, D., Atek, H., Tapken, C., 2008, *arXiv:0805.3601*